# Axial Dispersion Coefficients in Laminar Flows of Water-Distribution Systems

Pedro Romero-Gomez[1] and Christopher Y. Choi, A.M.ASCE[2]

**Abstract:** Because longitudinal dispersion is becoming increasingly germane to the problem of accurately determining water quality, water-resource managers and engineers seeking to represent solute transport in drinking-water systems must be able to compute relevant dispersion coefficients. Accordingly, the present study was undertaken to develop and experimentally verify a modified advection-dispersion-reaction transport equation as well as the formulas used to calculate the axial dispersion coefficient. The analysis assumes laminar flows, constant mean velocities, and short travel times (dimensionless time, $T < 0.01$). With regard to the modified transport equation, the dispersion term was assumed to be direction-dependent. Thus, two distinct dispersion rates (forward and backward) were recognized and quantified as opposed to the single value used in conventional dispersion models. With the dimensionless travel time taken to be the independent variable, the developed dispersion coefficients increased at about one-fourth of the growth rate exhibited by the conventional dispersion formula. The proposed scheme demonstrated a large improvement over the conventional formula when its performance was judged against experimental runs using various combinations of pipe lengths, tracer injections, mean flow velocities, and solute properties. This study's findings should lead to accurate water-quality predictions and corresponding quantitative risk assessments, especially in pressure zones where low-speed flows prevail. **DOI: 10.1061/(ASCE)HY.1943-7900.0000432.** © *2011 American Society of Civil Engineers.*

**CE Database subject headings:** Dispersion; Water distribution systems; Optimization; Water quaty; Laminar flow.

**Author keywords:** Axial dispersion; Dispersion rate; Optimization; Water quality.

## Introduction

Water-resources managers and engineers utilize computational tools not only to assess the status of hydraulic and water-quality conditions over large drinking-water distribution systems, but also to design utility expansions. The primary engines of these tools are the mathematical models that describe the underlying transport mechanisms used to move water (hydraulic) and solutes (water quality) through the system's various components. Currently, most of these quality solvers are on the basis of the assumption that solutes do not spread as they travel along a pipe, i.e., axial dispersion is neglected. This assumption postulates that flows in pressurized systems are highly turbulent and that such turbulence promotes a strong advective solute transport, one that prevails over longitudinal dispersion. However, a refinement of all-pipe hydraulic models has revealed a wide range of conditions, ranging from turbulent flows through mains and transmission lines (Blokker et al. 2010) to intermittent or even stagnant flows in service lines, which are laminar in nature (Buchberger et al. 2003). For quantitative risk assessment, in particular, the extended exposure duration because of axial dispersion is critical for the estimation. Therefore, the present study aims at quantifying dispersion rates under such low-flow conditions.

Researchers originally accounted for axial dispersion by first expanding the one-dimensional advection-reaction model (1D-AR) currently in use and then turning it into a 1D-advection-dispersion-reaction (1D-ADR) equation capable of predicting quality parameters with higher accuracy. This modeling expansion spurred the development of efficient and accurate numerical solutions to the 1D-ADR equation, which could be applied to real-size water systems (Islam and Chaudhry 1998; Tzatchkov et al. 2002; Basha and Malaeb 2007). Another set of studies is related to developing dispersion coefficients ($E$) involved in the aforementioned formulations; Taylor (1953) first developed analytical solutions and corresponding experimental validations to quantify steady-state dispersion rates ($E^*$) in capillary tubes under constant flows. When scaled up to match the sizes of pipes and flows typically found in municipal water-distribution systems, Taylor's model only applies in the unlikely event that the residence time in a single pipe reaches the order of days. Given that the dispersion rate is not constant but transient, Gill and Sankarasubramanian (G-S 1970) found an expression for the dispersion coefficient that increases with respect to travel time and asymptotically approaches the value calculated using Taylor's formula, $E^*$. The implementation of the G-S (1970) coefficient into the 1D-ADR equation is complex because it involves a sum of Bessel functions; thus, Lee (2004) provided a simplified form that performs well for long (but not for short) travel times ($T > 0.01$, see Eq. (1)).

Other studies have used computational fluid dynamics (CFD) tools to examine axial dispersion in pipe flows. For instance, Ozdemir and Ger (1999) analyzed transient chlorine transport with decay rates through CFD and verified the model results experimentally. Ekambara and Joshi (2004) carried this work further by simulating flows over a wide range of Peclet numbers and dimensionless times with acceptable experimental/numerical confirmations. Romero-Gomez et al. (2008) evaluated CFD models and experimental runs for various Reynolds numbers in the laminar,

[1]Graduate Research Assistant, Dept. of Agricultural and Biosystems Engineering, The Univ. of Arizona, Tucson, AZ 85721 (corresponding author). E-mail: pedromer@E-mail:.arizona.edu

[2]Professor, Dept. of Agricultural and Biosystems Engineering, The Univ. of Arizona, Tucson, AZ 85721. E-mail: cchoi@arizona.edu

Note. This manuscript was submitted on May 5, 2010; approved on March 29, 2011; published online on March 31, 2011. Discussion period open until April 1, 2012; separate discussions must be submitted for individual papers. This paper is part of the ***Journal of Hydraulic Engineering***, Vol. 137, No. 11, November 1, 2011. ©ASCE, ISSN 0733-9429/2011/11-1500–1508/$25.00.



Downloaded 09 Jan 2012 to 128.196.123.149. Redistribution subject to ASCE license or copyright. Visit http://www.ascelibrary.org

transitional, and turbulent flow regimes, and Romero-Gomez et al. (2009) further defined and validated the CFD setup upon which the present study is based.

The objective of the present study is to develop and experimentally validate an axial dispersion model for representing the spread of solute in constant laminar flows at short travel times ($T < 0.01$, see Eq. (1)). This analysis forms the foundation for further examining solute transport under more complex configurations. Axial dispersion under low-speed, steady-state flow conditions is the basis for analyzing stagnant and intermittent flows that often occur in the peripheral zones of piping systems (Buchberger et al. 2003). Furthermore, solutes take considerably less time to move along pipes in drinking-water systems than the time they need to reach the steady-state dispersion rate ($E^*$) introduced by Taylor (1953).

The present study began with a series of solute-dispersion experiments in pipes of 400–800 diameters of length in which the inlet concentration/flow conditions (experimental input data) gave rise to a concentration pulse at the pipe outlet. Next, these same experimental input data were fed into CFD simulations to thoroughly map out the spatiotemporal solute distribution along the pipe. When an acceptable agreement between the two approaches was achieved, the CFD technique then became a feasible way to characterize the axial dispersion rate, $E(T)$, as a function of travel time. Further verifications of the developed model determined its ability to represent axial dispersion in laminar pipe flows. To generalize our findings, we performed the analysis in terms of the following dimensionless parameters: (i) dimensionless pipe length ($x^*$) to define the location of solute migration, $L$, with respect to the pipe diameter, $d$; (ii) Reynolds number ($\mathsf{R}$) to account for the mean flow velocity's ($u_m$) geometric dimensions ($d$) and conveying fluid properties (kinematic viscosity, $\nu$); and (iii) Schmidt number ($\mathsf{Sc}$) to accommodate the solute properties (solute diffusion coefficient, $D_{\mathrm{AB}}$). Ultimately, the dimensionless travel time ($T$) combines all these parameters and dictates the extent to which the dispersion coefficient has elapsed toward reaching steady-state conditions:

$$x^* = \frac{L}{d}; \qquad \mathsf{R} = \frac{u_m d}{\nu}; \qquad \mathsf{Sc} = \frac{\nu}{D_{\mathrm{AB}}}; \qquad \bar{t} = \frac{L}{u_m}$$
$$T = \frac{4D_{\mathrm{AB}}\bar{t}}{d^2} = 4\frac{x^*}{\mathsf{Sc}\cdot\mathsf{R}} \tag{1}$$

## Prevalence of Laminar Flows and the Need for a Comprehensive Model

To assess the prevalence of low-flow conditions in water-supply systems, Buchberger et al. (2003) defined the dead-ends as those pipes that have only one connection to the primary looped portion of the network. In a dead-end, water flows in one direction only, i.e., from the entrance to the user. They found that dead-ends are very common in suburban and peripheral zones, as shown by a random sample taken from service zones in the cities of Cincinnati and Milford, OH, in which 23% and 35% of the total water-main length could be considered dead-end, respectively. They also found that dead-end pipes were characterized by random, intermittent, laminar-type flows throughout the day.

Blokker et al. (2010) conducted a tracer test (NaCl) in a water network with 10 km of mains serving 1,000 homes, 2 hotels, and 30 commercial properties in the Dutch town of Zandvoort, Netherlands. The primary purpose of the study was to evaluate two demand-allocation models through flow measurements and water age at four locations in the network. The Reynolds numbers over the network ranged from laminar to transitional to turbulent flows. This study demonstrated the difficulty of achieving reasonable prediction results on the basis of the plug flow model and using either of the demand-allocation models in an all-pipe hydraulic simulation. In response to a 3-h tracer injection at the booster station, the model predicted a pulse of 2.5 h at the furthest measurement location, whereas recordings showed a pulse that lasted 9 h. This discrepancy clearly demonstrates the need for a comprehensive and accurate axial dispersion model.

As part of this study, we surveyed the percentile of pipes that convey laminar flows over a pressure zone in the drinking-water system of Tucson, AZ. The zone covered an area of approximately 35.4 km by 29 km in the south-north and east-west directions, respectively. The hydraulic model contained 38 reservoirs, five tanks, 1,703 pipes, and 1,265 nodes under demands subject to a time-varying pattern obtained from the peak month of 2005. We used an EPANET toolkit/C++ routine to perform hydraulic simulations (time step = 1 h, duration = 96 h) and obtained mean flow velocities for each pipe on the basis of two methods: (a) all transient velocity values were averaged out and (b) the velocity values of the 25th percentile were averaged out. The findings revealed that 6% and 16% of the pipes carry laminar flows ($\mathsf{R} \le 2{,}100$) on the basis of methods a and b, respectively. Because the hydraulic model was skeletonized, we expect these percentiles to increase if all pipes were included. This showed the importance of examining solute transports under low-flow velocities that generally exacerbate axial dispersion.

## Experimental Technique

The experimental setup was constructed at the Real-Time Sensor Testing Laboratory of the Water Village, an experimental facility at the University of Arizona, Tucson, AZ. Fig. 1 depicts the components of the water-conditioning system and the main pipe section. Municipal tap water was run through five water filters connected in series to remove particles of sequentially decreasing sizes: 20 $\mu$m (FXWTC carbon filter, GE Company, Louisville, KY), 1 $\mu$m (Hytrex GX01-10, GE Company, Minnetonka, MN), 0.65 $\mu$m, 0.2 $\mu$m, and 0.04 $\mu$m (Clariflow 25-10320, Parker Hannifin Corp., Oxnard, CA). Following filtration, a reverse-osmosis system (GE Merlin, GE Company, Hollywood, FL) removed most of the salts contained in the tap water (about 90%) and increased the efficiency of an additional two-tank deionizer unit (Culligan International Company, Northbrook, IL). In this way, the water-conditioning system lowered the background conductivity from a range of 500–600 $\mu\mathrm{S\,cm^{-1}}$ to less than 20 $\mu\mathrm{S\,cm^{-1}}$ so that only the salt tracer injected into the pipe section affected the conductivity sensor readings.

A frequency inverter (L100-004MFU2, Hitachi Ltd., Chiba, Japan) controlled the centrifugal pump (1MS1C5E4, ITT Corp., Auburn, NY) that delivered water from the main source into a PVC pipe [15.6 mm diameter, 12.7 mm (1/2 in.) nominal diameter]. A programmable peristaltic pump (Tandem 1081, SciLog Inc., Middleton, WI) injected pulses of tracer solution drawn from a beaker. The tracer injection did not increase the main flow rate significantly (1–2% increase for short time periods). A turbine-type flow sensor (FTB602B-T, Omega Corp., Stamford, CT) measured the flow rates, which were controlled with a needle valve. The flow sensor had an accuracy of $\pm 1\%$ over a range of 0.3–9 L $\mathrm{min^{-1}}$ and was calibrated before each use. A static mixer (1/2-40C-4-12-2, Koflo Corp., Cary, IL) homogenized the tracer's distribution over the cross section of the pipe. A flow straightener eliminated swirls and distortions created by the mixer and induced the parabolic velocity distribution to develop more quickly. A four-ring



Downloaded 09 Jan 2012 to 128.196.123.149. Redistribution subject to ASCE license or copyright. Visit http://www.ascelibrary.org

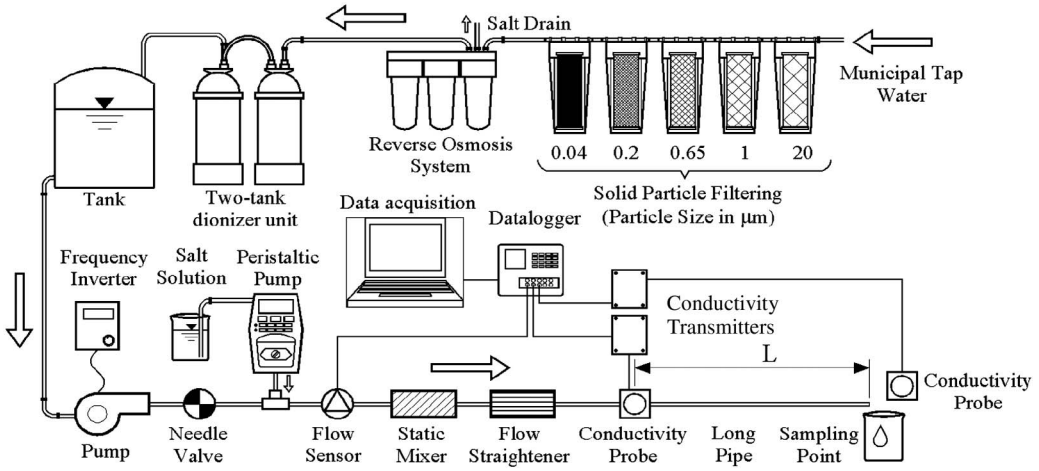



**Fig. 1.** Experimental setup for axial dispersion experiments through a straight pipe in laminar flow regime

potentiometric probe, combined with a conductivity transmitter (models CDE-1201 and CDTX1203, respectively, Omega Corporation, Stamford, CT) measured the inlet conductivity data. The accuracy was $\pm 2\%$ of the full range (0–1,999 $\mu$S cm$^{-1}$). Another unit was used to measure the conductivity values of grab samples taken at the downstream detection point. These sensors were first calibrated at two points using commercially available solutions (CDSA-1500, Omega Corp., Stamford, CT). Next, sensor readings of various tracer solutions determined the relation between conductivity and salt concentration. Flow rates and upstream solute concentrations were recorded every second using a data logger (CR23X Micrologger, Campbell Scientific, Logan, UT).

The development of the axial dispersion model was on the basis of a set of experimental runs that targeted Reynolds numbers ranging from 1,300 to 2,000 at intervals of 100 in a 6.5-m-long pipe ($x^* = 416$) and subject to 10 second-long injection pulses (Table 1). Table 2 lists the experimental runs used for verifying the developed model in both a 6.5 m- and a 12.5 m-long pipe ($x^* = 416$ and $x^* = 801$, respectively).

## Computational Fluid Dynamics Approach

The experimental runs supplied the flow rate and inlet concentration data needed to simulate the solute mass transport using CFD techniques. The approach consisted of numerically solving a set of conservation equations that fully describe the velocity field and solute distribution in pipe flows under prescribed initial/boundary conditions. The CFD approach was computationally intensive and we had to complete the following three steps to describe the detailed behavior of solutes moving along the pipe:

(i) Preprocessing—the pipe geometry was represented as a two-dimensional (2D), axisymmetric rectangle (area was $a \times L$, pipe radius by pipe length, respectively). The boundary types at the rectangle edges were velocity inlet (left), outflow (right), wall (top), and axis (bottom).

(ii) Numerical setup—a field function of the conventional parabolic velocity profile was applied over the domain. This assumption eased the computational expense to solving only the transient species-transport equation for laminar flows:

$$\frac{\partial}{\partial t}(\rho C_i) + \nabla \cdot (\rho \bar{u} C_i) = \nabla \cdot (\rho D_{\mathrm{AB}}) \nabla C_i \qquad (2)$$

As the formula states, the transient change (the first term) of the solute concentration at the cell node $i(C_i)$ is the result of the convection flux (the second term) induced by local velocities ($\bar{u}$) and the diffusive solute transport resulting from concentration gradients (the last term). Solute (NaCl) was assumed to be conservative with $D_{\mathrm{AB}} = 1.2 \times 10^{-9}$ m$^2$ s$^{-1}$. The water density ($\rho$) setting was 998 kg m$^{-3}$. The inlet boundary condition for the transport equation was equal to the measured inlet concentration at the upstream sensor in a uniform radial profile. Such a condition is applicable because the

**Table 1.** Description of Experimental Runs for Verifying CFD Simulations

| Reynolds number (target) | Reynolds number (measured) | Mean flow velocity ($u_m$), m s$^{-1}$ | Dimensionless time ($T$), $10^3$ |
|---|---|---|---|
| 1,300 | 1,281 | 0.083 | 1.552 |
| 1,400 | 1,387 | 0.089 | 1.434 |
| 1,500 | 1,516 | 0.098 | 1.312 |
| 1,600 | 1,585 | 0.102 | 1.255 |
| 1,700 | 1,705 | 0.110 | 1.166 |
| 1,800 | 1,796 | 0.116 | 1.107 |
| 1,900 | 1,903 | 0.123 | 1.045 |
| 2,000 | 1,997 | 0.129 | 0.996 |

Note: Mean flow velocities and resulting dimensionless times are calculated for a pipe diameter of 15.6 mm [12.7 mm (1/2 in.) nominal diameter].

**Table 2.** Description of Experimental Runs for Verifying the Developed Axial Dispersion Model

| Reynolds number (measured) | $x*$ | Injection duration (s) | Initial dispersion rates, $10^3$ m$^2$ s$^{-1}$ | | Shown in figure |
|---|---|---|---|---|---|
| | | | $E_b(0)$ | $E_f(0)$ | |
| 1,479 | 801 | 10 | 0.0 | 0.0 | 5 |
| 1,493 | 801 | 60 | 1.5 | 0.0 | 6 |
| 1,497 | 416 | 10 | 7.3 | 3.8 | 5 |
| 1,596 | 416 | 10 | 8.0 | 4.0 | 5 |
| 1,620 | 801 | 10 | 0.0 | 0.0 | 5 |
| 1,727 | 416 | 10 | 8.0 | 4.0 | 5 |
| 1,750 | 801 | 10 | 1.0 | 0.0 | 5 |
| 1,893 | 801 | 60 | 0.0 | 0.0 | 6 |

Note: Initial dispersion rates for simulating each case are also listed. Outcomes are shown in the figures referred to in the last column



Downloaded 09 Jan 2012 to 128.196.123.149. Redistribution subject to ASCE license or copyright. Visit http://www.ascelibrary.org

mixer guarantees that concentrations are uniform at the start of the pipe section.

(iii) Postprocessing—the flow-rate-weighted average ($C_D$) of cell center concentrations ($C_k$) at location $x_j$ and time $t_i$ was calculated as follows:

$$C_D(x_j, t_i) = \frac{2}{a^2 u_m} \sum_{k=1}^{N} u_k C_k r_k \Delta r_k \tag{3}$$

in which $u_k$ = local axial velocity at the cell center; $r_k$ = cell center's distance to the pipe centerline; $\Delta r_k$ = cell size in the radial direction; and $u_m$ = mean flow velocity. The concentration time series at various distances, $C_D(x_j, t_i)$, established the baseline for deriving the dispersion rates included in the 1D-ADR model. Furthermore, the flow-rate-weighted average physically corresponded to the solute concentration of the bulk grab sample collected at the pipe outlet.

The CFD simulations of axial dispersion in pipes were performed using a finite-volume-based solver. Romero-Gomez et al. (2009) provided details on the preanalysis of the numerical setup used in the present study as well as its benchmarking against experimental data obtained by Taylor (1953). The preanalysis determined the nonuniform mesh size, discretization scheme, and time step that would have no effect on the simulated solution to axial dispersion. The goal of the preanalysis was to minimize the likelihood of incorrect settings or erroneous assumptions. The resulting numerical setup contained 4,800 cells per 100 diameters of pipe length simulated with a second-order upwind scheme (Ansys Inc. 2009) at a time interval of 0.01 s. Approximately 30% of the cells pertained to the boundary-layer zone defined near the pipe wall, where large concentrations of gradients were expected.

## One-Dimensional Advection-Dispersion-Reaction Model

A feasible approach for modeling axial dispersion over large water systems requires the 1D-ADR model described as follows:

$$\frac{\partial C_S}{\partial t} = E \frac{\partial^2 C_S}{\partial x^2} - u_m \frac{\partial C_S}{\partial x} + k C_S \tag{4}$$

This model dictates that the rate of change of a transient solute concentration ($C_S$) at any location along the pipe (left-hand side) is the result of (i) the intermixing of mass between adjacent water volumes (dispersion, the first term on the right-hand side), (ii) the solute mass that the bulk flow conveys (advection, the second term on the right-hand side), and (iii) the growth or decay of the solute mass because of reactions within the bulk flow or along the pipe walls (reaction, the third term on the right-hand side). We neglected the reaction term because solutes in the experiments and simulations of this study are conservative. Whereas Taylor's formula (1953) for steady-state dispersion rates, ($E^*$, Eq. (5)) only applies for very long travel times ($T > 1/16$), Lee (2004) accounted for the transient nature of dispersion rates by applying Eq. (6):

$$E^* = \frac{a^2 u_m^2}{48 D_{AB}} \tag{5}$$

$$E(T) = E(0) \exp(-16T) + \beta(T) E^* \tag{6}$$

in which $E(0)$ = initial value of the dispersion rate; and $\beta(T) = 1 - \exp(-16T)$. However, Eq. (6) tends to amplify the dispersion effect at relatively short travel times ($T < 0.01$, Romero-Gomez et al. 2008). Furthermore, the presence of solute tailing long after a tracer pulse has passed a fixed downstream location reveals that the dispersive rate toward the end of the pulse is stronger than the rate near the front. Eqs. (5) and (6) establish that dispersion rates are affected by an averaged flow velocity uniformly distributed over the cross section. Nevertheless, low-velocity regions near the wall strongly hinder solute transport because of the nonslip boundary condition, not in equal magnitude as is the case in regions near the centerline. Consequently, a major assumption in our analysis is that applying the same dispersion rate in both directions will not fully represent the actual transport phenomena. In this respect, then, the present work departs from previous formulations by modifying the diffusion term in the 1D-ADR equation to accommodate the direction-dependent dispersion transport. Eq. (7) formalizes the fact that the difference between mass fluxes, backward and forward at a specific location, derives from the different dispersion rates driving solute transport ($E_b$ and $E_f$, respectively). In Eq. (7), the dispersion term shows a first-stage approximation using the finite-difference method to allow for the direction dependency of the dispersive transport.

$$\frac{\partial C_S}{\partial t} = \frac{1}{\Delta x}(\phi_b - \phi_f) - u_m \frac{\partial C_S}{\partial x} \tag{7}$$

in which

$$\phi = -E_b \left.\frac{\partial C}{\partial x}\right|_b \quad \text{and} \quad \phi_f = -E_f \left.\frac{\partial C}{\partial x}\right|_f$$

The transient form of $E(T)$ in Eq. (6) incorporates two components: an initial dispersion rate that decays exponentially over time and an increasing, instantaneous rate that becomes asymptotic to Taylor's dispersion rate ($E^*$) at long $T$ values. In following such a general formulation, the proposed dispersion models, $E_b$ and $E_f$, take this form:

$$\begin{aligned} E_b &= E_b(0) \exp(-16T) + \beta_b(T) E^* \quad \text{and} \\ E_f &= E_f(0) \exp(-16T) + \beta_f(T) E^* \end{aligned} \tag{8}$$

Initial coefficient values, $E_b(0)$ and $E_f(0)$, account for dispersion effects that were developing before the solute pulse was measured upstream, namely, dispersion occurring between the injection point and the upstream conductivity sensor. Such initial effects are expected to decay as $T$ progresses. The second term is almost linear at short time spans ($T < 0.01$), during which we can expect the coefficients $\beta_f$ and $\beta_b$ to be linear, although different from Lee's (2004). Parameters $\beta_f$ and $\beta_b$ are dimensionless, dependent on $T$, and represent the main focus of the present work, as shown subsequently.

The numerical solution to Eq. (7), subject to the following initial and boundary conditions, was computed using the unconditionally stable Crank-Nicholson scheme:

$$\text{Initial Condition } C_S(x, 0) = 0$$

$$\text{Boundary Conditions } C_S(0, t) = C_0(x); \qquad \left.\frac{\partial C_S}{\partial x}\right|_{x \to \infty} = 0$$

$$t > 0$$

This classical scheme is a combined explicit/implicit method because it predicts concentrations at time $t_{n+1}$ by accounting for both the current (at $t_n$) and future ($t_{n+1}$) concentration values in the solution process. Discretizing all the derivatives in Eq. (7) gave rise to a tridiagonal system of equations that was solved by applying the widely known Thomas algorithm. The value of $\Delta x$ was set equal to $u_m \cdot \Delta t$, in which the time step $\Delta t$ was equal to 1 s.



Downloaded 09 Jan 2012 to 128.196.123.149. Redistribution subject to ASCE license or copyright. Visit http://www.ascelibrary.org

## Partial-Differential-Equation-Constrained Parameter Optimization

The estimation of parameters ($E_f$ and $E_b$) of a mass transport phenomenon governed by a partial differential equation (PDE, Eq. (7)) is often called PDE-constrained parameter optimization. The proposed formulation sought to minimize the deviation between the solute concentrations predicted by the 1D-ADR equation ($C_S$, Eq. (7)) and the results obtained from the CFD simulations ($C_D$, Eq. (3)). The objective function is defined by Eq. (9) and dispersion coefficients $E_f$ and $E_b$ are the implicit decision variables. Eq. (9) places emphasis on the prediction of both the arrival time and the maximum downstream concentration (the power of the first term is 3, from time zero to the time when the maximum value of $C_D$ occurs, or $T_{\max}$) while accounting for the solute mass that lags behind after the maximum value is detected (second term, past $T_{\max}$):

$$\min z_j = \sum_{i=0}^{T\max} [|C_D(x_j, t_i) - C_S(x_j, t_i)|]^3 + \sum_{i=T\max+1}^{T\text{end}} [C_D(x_j, t_i) - C_S(x_j, t_i)]^2 \quad (9)$$

We applied Newton's method to minimize $z_j$, which is implicitly a function of two dispersion coefficients (through Eq. (7)) arranged in a vector, $\bar{E} = (E_f, E_b)$. The first step was to calculate the gradient of $z_j$ ($\nabla z_j$) and to evaluate it at the initial guess values ($\bar{E}_0$). Next, the Hessian matrix of $z_j$, $H(z_j)$, was also evaluated at $\bar{E}_0$, at which

$$\nabla z_j = \left(\frac{\partial z_j}{\partial E_f}, \frac{\partial z_j}{\partial E_b}\right) \quad (10)$$

$$H(z_j) = \begin{pmatrix} (\partial^2 z_j)/(\partial E_f^2) & (\partial^2 z_j)/(\partial E_f \partial E_b) \\ (\partial^2 z_j)/(\partial E_b \partial E_f) & (\partial^2 z_j)/(\partial E_b^2) \end{pmatrix} \quad (11)$$

Finally, the updated dispersion values were computed by subtracting the product of $\nabla z_j$ and the inversed Hessian matrix from the initially presumed value:

$$\bar{E}_n = \bar{E}_{n-1} - \nabla z_j(\bar{E}_{n-1}) \cdot \{H[z_j(\bar{E}_{n-1})]\}^{-1} \quad (12)$$

This iterative process continued until a prescribed error between the old ($n-1$) and updated ($n$) values was met. Newton's method typically requires a fairly accurate initial guess of the value to speed up convergence. This, however, does not represent a drawback because dispersion values were expected to monotonically increase from an initial dispersion estimate at the pipe entrance, as dictated by Eqs. (8). By solving this formulation at subsequent pipe intervals, we could infer how much the axial dispersion coefficients changed as a function of travel time and then we could obtain the dimensionless parameters $\beta_f$ and $\beta_b$ (in Eq. (8)) and further generalize the applicability of our findings to other scenarios.

## Results and Discussion

The first stage in the development of the axial dispersion model entailed validating the results from CFD simulations against the experimental readings of solute concentration in a 6.5-m-long pipe ($x^* = 416$). To accomplish this, we introduced a 10-s-long injection pulse of a sodium chloride solution at a flow rate equal to 30 mL min$^{-1}$. Multiple scenarios involving solute transport in the real world range from very gradual changes (e.g., chlorine leaving treatment facilities) to rapid quality disruptions (e.g., sudden contaminant ingresses). Short time pulses in the present experimental setup can be scaled up to pulses of minutes or hours in actual systems. Two benefits result from such cases. First, dispersion rates can be determined more accurately given that solute spread is prevalent and strong. Second, such cases could serve greatly to support tracer studies and sensor location optimization tools intended to improve water security. For instance, the time that elapses between any accidental or intentional introduction of a contaminant into a potable water system and its detection or public report is likely to be relatively short in comparison with the time spans associated with mild quality gradients resulting from operations.

Preliminary runs conducted by using an in-line conductivity sensor at the downstream location showed concentration curves consistently delayed with respect to the expected ones. CFD-simulated solute distributions over the cross section revealed that, although the mixer and flow straightener ensured a more uniform concentration profile for the upstream conductivity sensor to read, the large radial gradients developed at the pipe outlet reduced the downstream sensor's ability to accurately read and average out the bulk-flow values. Such a situation was also the reason preliminary attempts failed to determine accurate dispersion rates through the so-called frozen cloud approximations. A central assumption in the frozen cloud approach holds that radial mixing has fully developed and produced uniform profiles at both the entrance and end pipe locations, a condition not achieved during short time spans. For this reason, we collected grab samples to obtain flow-rate-weighted concentration values that were directly comparable to CFD results.

Another significant issue arose at the experimental stage of this work: the spread of the solute after it had traveled 6.5 m ($x^* = 416$) at low R numbers ($R < 1,300$) produced concentration measurements that became strongly affected by the sensor's lower conductivity limit. As a result, the tested Reynolds number ranged between 1,300 and 2,000. Nevertheless, the nondimensionalized analyses of our findings directly applied to the entire laminar flow regime, as is demonstrated in subsequent paragraphs. All experimental data points presented in this work were obtained with duplicate runs conducted at the same Reynolds number in order to guarantee repeatability during data collection.

Fig. 2 depicts the results obtained from all the approaches when the pulse migrated to the pipe end at $R = 1,516$. Although the inlet pulse lasted 10 s, the upstream readings spread as a result of the travel distance and the components (flow meter, mixer, and flow straightener) between the injection point and the upstream sensor.

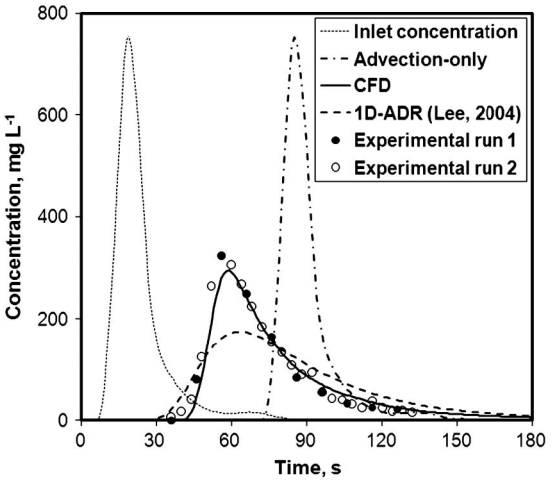



**Fig. 2.** Inlet concentration pulse traveling at $R = 1,516$ gives rise to transient concentrations at $x^* = 416$ by various approaches



Downloaded 09 Jan 2012 to 128.196.123.149. Redistribution subject to ASCE license or copyright. Visit http://www.ascelibrary.org

All downstream data featured lower peak values and a stretched curve in comparison to the upstream signal. Nevertheless, such expected characteristics were quantitatively distinct depending upon the approach. Among the four downstream curves, the CFD-simulated results and experimental results showed the highest correlation over time ($R_2 = 0.96$ for this R number in Fig. 3). Experimental errors might have occurred because each sample's collection was 4-s-long to attain the minimum volume required to fill the conductivity probes (at least 60 mL). However, the solute distribution in the outgoing flow changed continuously in both time and space, and the samples ultimately averaged out the concentration gradients. The CFD-simulated results, on the other hand, were only spatially averaged (see Eq. (3)).

The significant improvement in water-quality prediction achieved by using CFD becomes evident when compared against the outcomes obtained from 1D-ADR simulations using an existing dispersion model (Lee 2004) that magnified the dispersive effect, as shown by the shorter solute arrival time, the lower peak concentration, and the more stretched curve. Although previous evidence confirms the accuracy of this model when long travel times have elapsed, the present findings suggest the benefits of developing a more representative dispersion formula for short pipes ($T < 0.01$). The 1D advection-reaction (1D-AR) model exhibited the largest deviation against experimental observations because the delayed outlet concentrations basically mimic the shape of the upstream tracer injection.

The other experimental runs listed in Table 1 essentially replicated the aforementioned similarities and discrepancies occurring between the experimental and the CFD-simulated results, as depicted in the scattergrams in Fig. 3. The $x$-coordinate of each data point corresponds to the concentration reading at a specific time, and its $y$-coordinate corresponds to the CFD-predicted concentration. Each chart also shows the $R^2$ value and the number of data points included in the comparison ($N$). The CFD results slightly underpredicted peak concentrations for all cases excepting R = 1,796. The squared-correlation coefficient remains high for all the instances, with the lowest value for R being 1,796 ($R_2 = 0.81$) and the highest being 1,281 ($R_2 = 0.97$). These plots further demonstrate the ability of CFD tools to accurately represent the axial dispersion transport in pipe flows. Outcomes from 1D-ADR runs using the existing dispersion model (Lee 2004) reproduced the previously explained features as in R = 1,516, and thus are omitted from Fig. 3.

The CFD simulations made concentration time series available at any location for stepwise calculations of the dispersion coefficients. Because the case for R = 1,705 fell near the middle of the analyzed R number range, we selected it when we carried out the parameter optimization phase of this work. The optimization formulation (Eq. (9)) was applied over intervals $\Delta x^* = 32$ (for $x^* = 0$ to 960), $\Delta x^* = 64$ (for $x^* = 960$ to 1,600), and $\Delta x^* = 160$ (for $x^* = 1{,}600$ to 3,200). As seen, $\Delta x^*$ increased gradually as the formulation became less sensitive to $\Delta x^*$ at further distances from the pipe inlet. Fig. 4(a) depicts the linear evolution of the optimal dispersion coefficients as a function of travel time. In all instances, the backward dispersion rate ($E_b$) was greater than the forward value ($E_f$) by a practicably constant absolute difference ($E_b - E_f$) with an average equal to $5.3 \times 10^{-3}$ m$^2$ s$^{-1}$. In terms of percentiles, the forward dispersion rate ($E_f$) was lower than $E_b$ by 24% (at pipe entrance), decreasing monotonically to 1% (at pipe outlet). This finding indicates that the influence of both the initial values and the direction-dependence of dispersion rates is significantly stronger near the pipe entrance and lessens over longer travel times. The optimal coefficients did not produce a perfect agreement with the CFD-simulated concentrations at all the locations; instead, they yielded the least-possible error produced by the bidirectional dispersion model.

The curve-fitting of the optimal coefficients shown in Fig. 4(a) to models in Eq. (8) led to initial dispersion rates of $E_b(0) = 7.5 \times 10^{-3}$ m$^2$ s$^{-1}$ and $E_f(0) = 2.1 \times 10^{-3}$ m$^2$ s$^{-1}$, whereas the $\beta_b$ and $\beta_f$ coefficients turned out to be alike (Eq. (13)), as illustrated in Fig. 4(b). This finding dictates an eventual convergence of both the backward and forward dispersion rates over long travel times. The slope of Eq. (13) is 24.5% with respect to the $\beta$-coefficient found by Lee (2004) and confirmed the earlier findings obtained

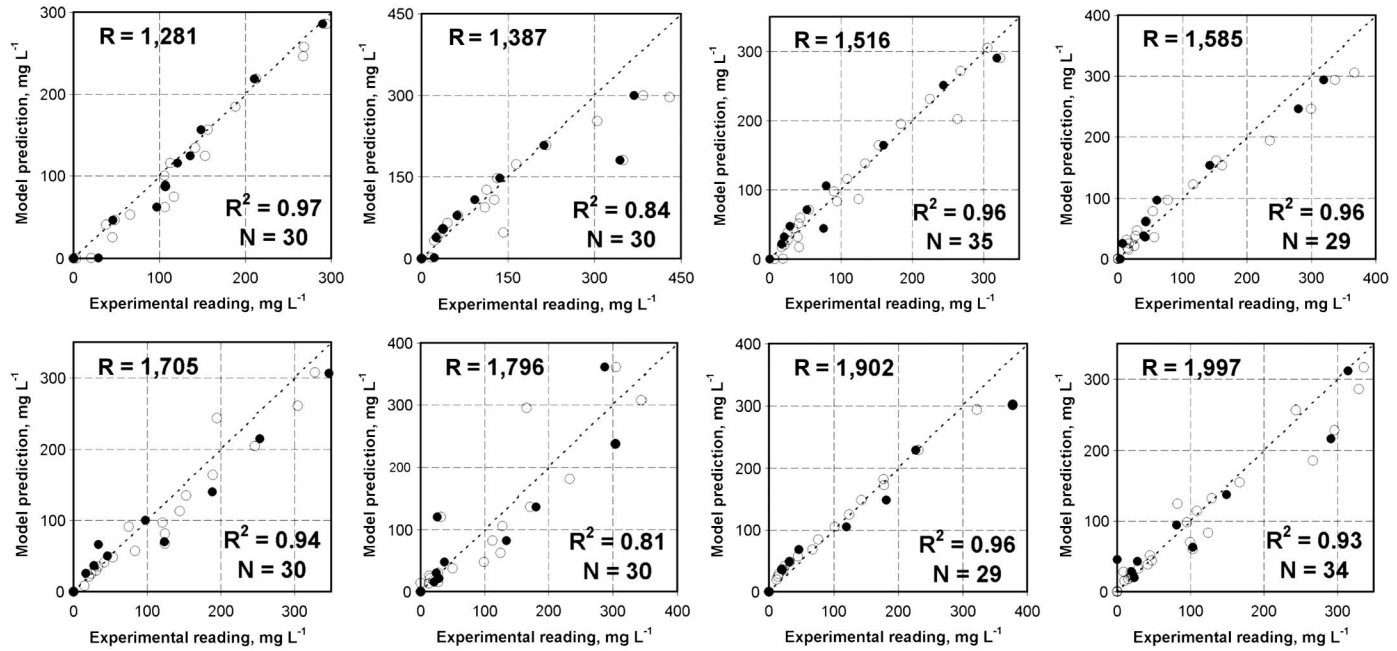



**Fig. 3.** Comparison of experimental (1st run, black circles; 2nd run, white circles) versus CFD-simulated concentrations at the downstream location ($x^* = 416$) for all tested Reynolds numbers



Downloaded 09 Jan 2012 to 128.196.123.149. Redistribution subject to ASCE license or copyright. Visit http://www.ascelibrary.org

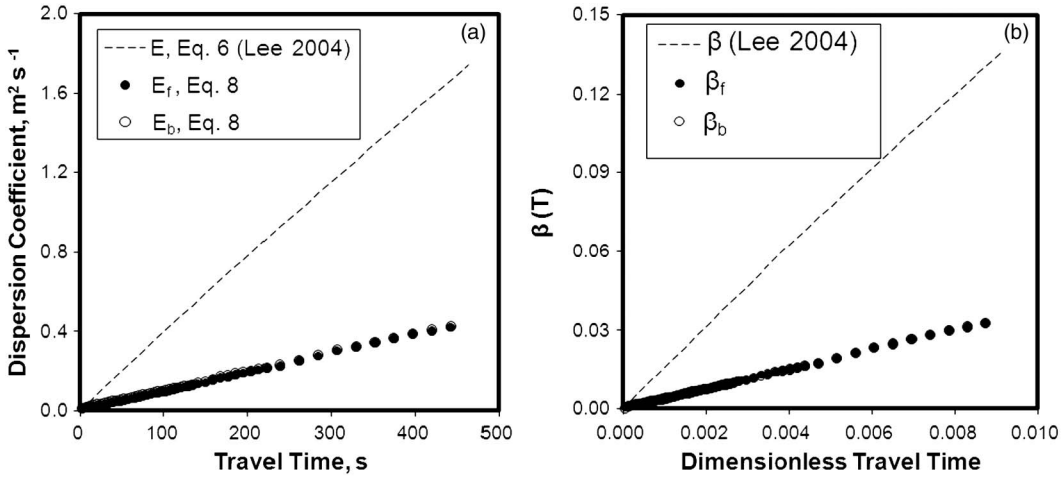



**Fig. 4.** (a) Dimensional and (b) dimensionless axial dispersion coefficients as a function of travel time for R = 1,705

by Romero-Gomez et al. (2008), in which the experimental dispersion rates calculated by the method of moments were 20–25% of those predicted by Lee's model:

$$\beta_f = \beta_b = \beta = 3.705T \tag{13}$$

The battery of experimental tests listed in Table 2 was run to verify the axial dispersion formula for solving various combinations of Reynolds number, pipe length, and injection duration. Fig. 5 illustrates the dispersion effect in a 6.5-m-long pipe ($x^* = 416$) and in a 12.5-m-long pipe ($x^* = 801$). As expected, the inlet pulse disperses considerably more at larger $x^*$ values. Fig. 5 exhibits an acceptable agreement between the experimental measurements and the 1D-ADR predictions made by the newly developed dispersion model. The largest discrepancies were observed at peak concentrations for runs at R = 1,727 and 1,750. These were underestimated by the modeling approach; however, this discrepancy is a consequence of the optimization formulation in which we primarily emphasized the model's ability to predict the solute arrival time over its ability to reproduce other features. The duplicate runs produced downstream-concentration readings that complemented each other.

Reducing the computational time needed for simulating the solute transport is another important aspect to consider when assessing enhanced modeling capabilities. Accordingly, we found that the

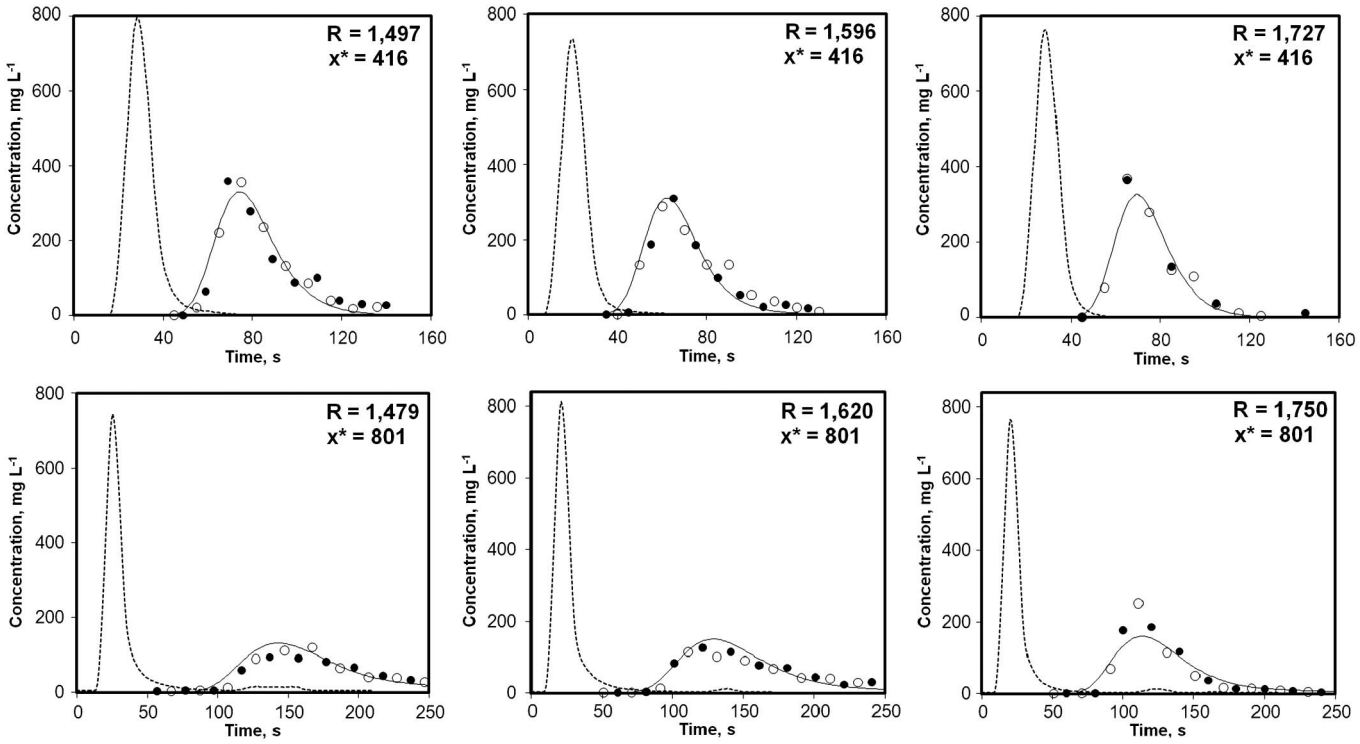



**Fig. 5.** Experimental verification of the developed axial dispersion coefficient model at various Reynolds numbers; the inlet concentration pulse (dotted line) gives rise to downstream concentrations at $x^* = 416$ and 801 by several approaches: 1D-ADR with dispersion rates developed in the present study (continuous line), 1D-ADR with dispersion rates by Lee (2004) (dashed line), and experimental measurements (1st run, black circles; 2nd run, white circles)



Downloaded 09 Jan 2012 to 128.196.123.149. Redistribution subject to ASCE license or copyright. Visit http://www.ascelibrary.org

completion of a single CFD simulation run conducted on a personal computer (with an Intel Core 2.33 GHz, 1.99 gigabytes of RAM) required 12 to 18 h, whereas the corresponding 1D-ADR run took less than 3 s on average using the same computer. It is expected that expedient numerical schemes that seek to efficiently solve the 1D-ADR equation for large piping networks (Tzatchkov et al. 2002; Basha and Malaeb 2007) will surely require much shorter simulation times.

As prescribed by Eq. (8) and the dimensionless parameter $\beta$ in Eq. (13), when a solute in one water parcel intermixes with adjacent volumes, the mixing becomes stronger in a quasi-linear fashion with respect to the travel time (or as a function of the reached length upon constant mean flow velocity, $u_m$). Axial dispersion is in fact a global phenomenon that results from the simultaneous, local mass transfers occurring at a microscale level, transfers such as (i) axial-diffusion transport because of large concentration gradients in the $x$-direction, (ii) local convective transfers occurring as bulk-flow motion takes place at different, radially distributed velocities, and (iii) radial diffusion spreading from the high-velocity center region of the pipe to act on the low-velocity pipe-wall region (at the front of the pulse and in inverse direction at the back of the pulse). Because the aforementioned processes take place irrespective of whether the solute is introduced in the main stream as a pulse or a continuous injection, we extended the experimental verification of the developed dispersion model to include long injection pulses (1 min duration).

Fig. 6 illustrates the evaluation of the model's performance during long injection runs (1 min) at two Reynolds numbers ($\mathsf{R} = 1{,}493$ and 1,893) in a 12.5-m-long pipe ($x^* = 801$). The model introduced in this study more accurately predicted downstream concentrations for $\mathsf{R} = 1{,}493$ than for $\mathsf{R} = 1{,}893$. It is also worth pointing out that the prediction error over the curve-tailing for the case $\mathsf{R} = 1{,}493$ was larger than in previous runs (Fig. 5). This larger error arises because the optimization formula penalizes, to a lesser extent, the differences spread over the tailing side of the curve (differences are squared in the second term of Eq. (9)).

The incoming and outgoing solute mass measured for each run and shown in Tables 1 and 2, was determined by calculating the definite integral under the concentration clouds through the trapezoidal rule. The mass balance for each run was equal to the outgoing total mass divided by the incoming total mass. The averaged mass balance for runs used in model development (Table 1) was $98.0 \pm 4.9\%$, whereas that of the experimental runs for model validation (Table 2) was $100.5 \pm 4.2\%$. Such averages show that there was no significant solute loss because of salt settling and that experimental findings confirmed the nonreactive transport of the salt tracer.

The developed dispersion model can be applied to situations involving dimensionless travel times ($T$) smaller than 0.01. This limit derives from the time span over which the parameter-optimization procedure was applied. To translate this model limitation within the context of pipe diameters and solutes of interest for drinking-water utilities, Table 3 shows the pipe lengths

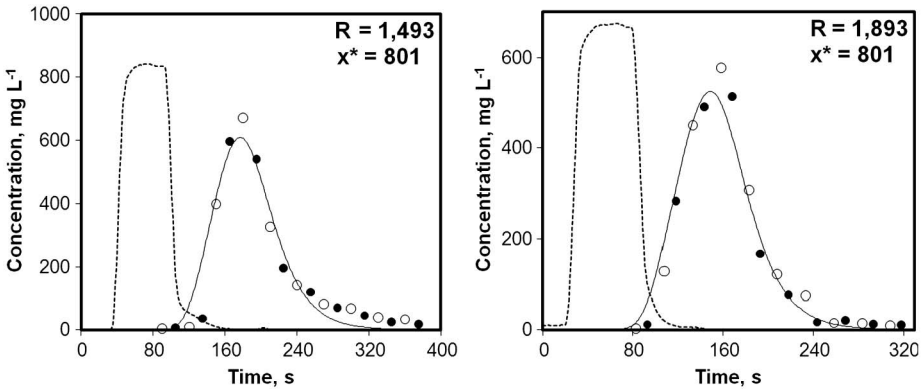



**Fig. 6.** Experimental verification of the developed axial dispersion coefficient model at two Reynolds numbers with long injection pulses (1 min); the inlet concentration pulse (dotted line) gives rise to downstream concentrations at $x^* = 801$ by various approaches: 1D-ADR with dispersion rates developed in the present study (continuous line), 1D-ADR with dispersion rates by Lee (2004) (dashed line), and experimental measurements at $L = 12.5$ m (1st run, black circles; 2nd run, white circles)

**Table 3.** Pipe Lengths in Meters over which the Developed Dispersion Model Applies upon Flows of $\mathsf{R} = 500$ (Lower Bound) and $\mathsf{R} = 2{,}000$ (Upper Bound)

| | | Nominal pipe diameter (cm) | | | | | |
|---|---|---|---|---|---|---|---|
| Solute | $D_{AB} \times 10^9$ ($m^2\,s^{-1}$) | 1.27 | 2.54 | 5.08 | 10.16 | 15.24 | Sc |
| Free chlorine ($Cl_2$) | 1.38[a] | 11.6/46.2 | 23.1/92.5 | 46.2/185.0 | 92.5/370.0 | 138.7/554.9 | 728.3 |
| Sodium fluoride (NaF) | 1.39[b] | 11.5/45.9 | 23.0/91.8 | 45.9/183.6 | 91.8/367.3 | 137.7/550.9 | 723.0 |
| Monochloramine ($NH_2Cl$) | 1.88[c] | 8.5/33.9 | 17.0/67.9 | 33.9/135.8 | 67.9/271.6 | 101.8/407.3 | 534.6 |
| Sodium chloride (NaCl) | 1.53[d] | 10.4/41.7 | 20.9/83.4 | 41.7/166.8 | 83.4/333.7 | 125.1/500.5 | 656.9 |
| Mean flow velocity ($cm\,s^{-1}$) | | 3.96/15.83 | 1.98/7.91 | 0.99/3.96 | 0.49/1.98 | 0.33/1.32 | |
| Nominal pipe diameter (cm [in.]) | | 1.27 (½) | 2.53 (1) | 5.08 (2) | 10.16 (4) | 15.24 (6) | |

[a]Chang and Myerson (1985).
[b]Kau et al. (1999).
[c]Cochran et al. (2000).
[d]Tang and Sandall (1985).



Downloaded 09 Jan 2012 to 128.196.123.149. Redistribution subject to ASCE license or copyright. Visit http://www.ascelibrary.org

over which the model applies when assuming laminar Reynolds numbers of 500 and 2,000. Free chlorine ($Cl_2$), sodium fluoride (NaF), and monochloramine ($NH_2Cl$) are commonly used as disinfectants in municipal water systems in the United States. Sodium chloride (NaCl) is included because it was used as a tracer in the present work. As can be seen in Table 3, the pipe length over which the model applies is inversely proportional to the molecular diffusion coefficient and directly proportional to both the pipe diameter and flow Reynolds number (R).

The present modeling advancement establishes a foundation for future research that is needed to accurately predict water quality in real-world systems by accounting for dispersion. First, and as mentioned in the discussion on the prevalence of laminar conditions, transient dispersion in steady-state flows requires further analysis of solute transport in time-varying hydraulics. For instance, Lee (2004) demonstrated through linear system analysis that dispersion under an arbitrary sequence of laminar flow pulses is an extension of the steady-state hydrodynamic condition. Lee (2004) found that the rate of solute spread is greater in intermittent flows than it is in steady-state flows, given the same time-averaged flow rate. Thus, this study delivers accurate and validated dispersion rates on which further analyses similar to Lee's (2004) can be conducted. Second, the present model exhibits the sensitivity of dispersion predictions to initial dispersion rates in short pipes. Thus, a major challenge is to quantify the initial dispersion rates that may be strongly related to the solute mixing that occurs as the water flows through the pipe's components (flow sensor, mixer, and flow straightener) before arriving at the upstream measuring point. The initial dispersion can be studied experimentally as well as through modeling. In the present study, CFD outcomes provided guidance for establishing the values for $E_b(0)$ and $E_f(0)$ that were used in the model verification phase (Table 2). The findings consistently show that no impact from the mixer and flow straightener is manifest other than for determining the initial dispersion rate.

## Conclusions

In this study, we numerically examined and experimentally verified the axial dispersion of solutes traveling in laminar pipe flows. As a result of this work, we were able to develop a new formula for dispersion rates and incorporate it into a proposed, direction-dependent transport equation. On the basis of our subsequent verification runs, we can conclude that such an equation is a plausible way to evaluate, within feasible computational times, the water-quality parameters of a drinking-water distribution system. We found that, over short time spans, the dispersion rates behave in a quasi-linear manner as a function of travel time, with a slope that is about 25% of that dictated by existing formulas. Because we defined the model in terms of dimensionless variables, it can accommodate a wide variety of practically achievable combinations of flow rates, pipe diameters, and solute properties, as long as the flow regime remains laminar and the dimensionless travel time ($T$) is less than 0.01. The verification runs ascertained the applicability of the proposed model with respect to short and long upstream injections of solute. The outcomes of the present study further suggest that axial dispersion effects must be integrated into current water-quality solvers, which presently oversimplify the transport of nonreactive solutes, reducing it to an advection-only mode.

Because the hydraulic and water quality behavior in piping networks is complex and highly transient, the developed model may also serve as a starting point for determining dispersion coefficients under unsteady and intermittent flows in pipe systems. The methodology pursued in this study could also be used to extend the analysis to include transitional and turbulent flows and in so doing address the spectrum of conditions that are likely to be found in drinking-water systems. Furthermore, future research, we believe, should seek to combine the proposed dispersion model with the more efficient numerical schemes that are used to analyze large-size networks, and then this new dispersion model should be verified by means of field testing.

## Acknowledgments

This work is supported by the EPA/Department of Homeland Security (under grant no. 613383D). We would like to acknowledge collaborators Dr. Steve G. Buchberger and Dr. Zhiwei Li at the University of Cincinnati as well as Mirjam Blokker at KWR in the Netherlands. The following students contributed their valuable time during the experimental phase of this work: Ryan G. Austin, Mario Mondaca, Malorie Teich, Fernando Rojano, and Alex Andrade.

## References

Ansys Inc. (2009). *Ansys fluent 12.0 theory guide*, Canonsburg, PA.

Basha, H. A., and Malaeb, L. N. (2007). "Eulerian-Lagrangian method for constituent transport in water distribution networks." *J. Hydraul. Eng.*, 133(10), 1155–1166.

Blokker, E. J. M., Vreeburg, J. H. G., Beverloo, H., and Klein, A. M. (2010). "A bottom-up approach of stochastic demand allocation in water quality modeling." *Drinking Water Eng. Sci.*, 3(1), 43–51.

Buchberger, S. G., Carter, J. T., Lee, Y., and Schade, T. G. (2003). "Random demands, travel times and water quality in deadends," *AWWARF Rep. 90963F*, American Water Works Association, Denver.

Chang, Y. C., and Myerson, A. S. (1985). "The diffusivity of potassium chloride and sodium chloride in concentrated, saturated, and supersaturated aqueous solutions." *AIChE J.*, 31(6), 890–894.

Cochran, W. L., McFeters, G. A., and Stewart, P. S. (2000). "Reduced susceptibility of thin Pseudomonas aeruginosa biofilms to hydrogen peroxide and monochloramine." *J. Appl. Microbiol.*, 88(1), 22–30.

Ekambara, K., and Joshi, J. B. (2004). "Axial mixing in laminar pipe flows." *Chem. Eng. Sci.*, 59(18), 3929–3944.

Gill, W. N., and Sankarasubramanian, R. (1970). "Exact analysis of unsteady convective diffusion." *Proc. R. Soc. London, Ser. A*, 316(1526), 341–350.

Islam, M. K., and Chaudhry, M. H. (1998). "Modeling of constituent transport in unsteady flows in pipe networks." *J. Hydraul. Eng.*, 124(11), 1115–1124.

Kau, P. M. H., Binning, P. J., Hitchcock, P. W., and Smith, D. W. (1999). "Experimental analysis of fluoride diffusion and sorption in clays." *J. Contam. Hydrol.*, 36(1–2), 131–151.

Lee, Y. (2004). "Mass dispersion in intermittent laminar flow." Ph.D. dissertation, Univ. of Cincinnati, Cincinnati.

Ozdemir, O. N., and Ger, A. M. (1999). "Unsteady 2-D chlorine transport in water supply pipes." *Water Res.*, 33(17), 3637–3645.

Romero-Gomez, P., Li, Z., Choi, C. Y., and Buchberger, S. G. (2009). "Axial dispersion coefficients for laminar flows in water distribution systems." *Proc., World Environmental and Water Resources Congress*, ASCE, Reston, VA, 1–10.

Romero-Gomez, P., Li, Z., Choi, C. Y., Buchberger, S. G., Lansey, K. E., and Tzatchkov, V. T. (2008). "Axial dispersion in pressurized pipes under various flow conditions." *Proc., 10th Annual Water Distribution Systems Analysis Symp.*, ASCE, Reston, VA.

Tang, A., and Sandall, O. C. (1985). "Diffusion coefficient of chlorine in water at 25–60 degree C." *J. Chem. Eng. Data*, 30(2), 189–191.

Taylor, G. (1953). "Dispersion of soluble matter in solvent flowing slowly through a tube." *Proc. R. Soc. London, Ser. A*, 219(1137), 186–203.

Tzatchkov, V. G., Aldama, A. A., and Arreguin, F. I. (2002). "Advection-dispersion-reaction modeling in water distribution networks." *J. Water Resour. Plann. Manage.*, 128(5), 334–342.



Downloaded 09 Jan 2012 to 128.196.123.149. Redistribution subject to ASCE license or copyright. Visit http://www.ascelibrary.org